Squeezed-Light Enhancement and Backaction Evasion in a High Sensitivity Optically Pumped Magnetometer

C. Troullinou,[1,*] R. Jiménez-Martínez,[1] J. Kong,[2,†] V. G. Lucivero,[1] and M. W. Mitchell[1,3]
[1]ICFO - Institut de Ciències Fotòniques, The Barcelona Institute of Science and Technology, 08860 Castelldefels (Barcelona), Spain
[2]Department of Physics, Hangzhou Dianzi University, 310018 Hangzhou, China
[3]ICREA - Institució Catalana de Recerca i Estudis Avançats, 08010 Barcelona, Spain

(Received 4 August 2021; revised 31 August 2021; accepted 16 September 2021; published 2 November 2021)

We study the effect of optical polarization squeezing on the performance of a sensitive, quantum-noise-limited optically pumped magnetometer. We use Bell-Bloom (BB) optical pumping to excite a ^{87}Rb vapor containing 8.2×10^{12} atoms/cm^3 and Faraday rotation to detect spin precession. The sub-pT/$\sqrt{\text{Hz}}$ sensitivity is limited by spin projection noise (photon shot noise) at low (high) frequencies. Probe polarization squeezing both improves high-frequency sensitivity and increases measurement bandwidth, with no loss of sensitivity at any frequency, a direct demonstration of the evasion of measurement backaction noise. We provide a model for the quantum noise dynamics of the BB magnetometer, including spin projection noise, probe polarization noise, and measurement backaction effects. The theory shows how polarization squeezing reduces optical noise, while measurement backaction due to the accompanying ellipticity antisqueezing is shunted into the unmeasured spin component. The method is compatible with high-density and multipass techniques that reach extreme sensitivity.

DOI: 10.1103/PhysRevLett.127.193601

Optically pumped magnetometers (OPMs) [1], in which an atomic spin ensemble is optically pumped [2] and its spin dynamics optically detected, are a paradigmatic quantum sensing technology with applications ranging from geophysics [3] to medical diagnosis [4] to searches for physics beyond the standard model [5]. OPMs are also a useful proving ground to test sensitivity enhancement techniques that may some day be applied to atomic clocks [6], gyroscopes [7], and co-magnetometers [8,9]. In these sensors two quantum systems—atoms and light—interact to produce the signal. Understanding and controlling the quantum noise in this interacting system is an outstanding challenge [10–13].

At high atomic densities that give high OPM sensitivity, quantum noise of both atoms and light is important [1]. Measurement backaction, including the effect of probe quantum noise on the spin system, becomes important in such conditions [14], making it unclear whether squeezing of the probe light [15–18], which reduces noise in one optical component while increasing it in another, can reduce total noise in a high-sensitivity OPM. In contrast to squeezed-light enhancement in low-density OPMs [19], high-density squeezed-light OPMs [20] have to date shown a trade-off of sensitivity vs quantum noise reduction [21,22], and a worsening of sensitivity due to probe squeezing [12].

To show that squeezing can indeed benefit a high-sensitivity OPM, we study a backaction evading measurement scheme based on Bell-Bloom (BB) optical pumping [23] and off-resonance probing. We model the quantum noise dynamics, including optical and spin quantum noise, and their interaction. We find that measurement backaction noise is shunted into a spin component that does not contribute to the signal. In this way the scheme almost fully evades measurement backaction noise, including that associated with squeezing. We predict and experimentally demonstrate that squeezing improves the sensitivity of the OPM above the response bandwidth of the magnetometer, without significantly increasing noise in any part of the spectrum. Squeezing is also observed to improve the measurement bandwidth [24], i.e., the frequency range over which the sensitivity is within 3 dB of its best value.

Our sensor achieves sub-pT/$\sqrt{\text{Hz}}$ sensitivity to low-frequency finite fields, comparable to that of the best scalar OPMs implemented with mm-sized [25] vapor cells and far better than previous squeezed-light enhanced OPMs [12,19,20]. The backaction evasion scheme is compatible with sub-fT/$\sqrt{\text{Hz}}$ methods including high-density [3] and multipass [26] techniques, as well as with pulsed gradiometry [27,28] and closed-loop [29] techniques for operation at Earth's field [30] and in unshielded environments [31]. The BB technique also gives a clear view of the relationships among different noise sources. The results provide experimental input to the much-discussed question of whether squeezing techniques can, in practice, improve the performance of atomic sensors [10–12,22,32].

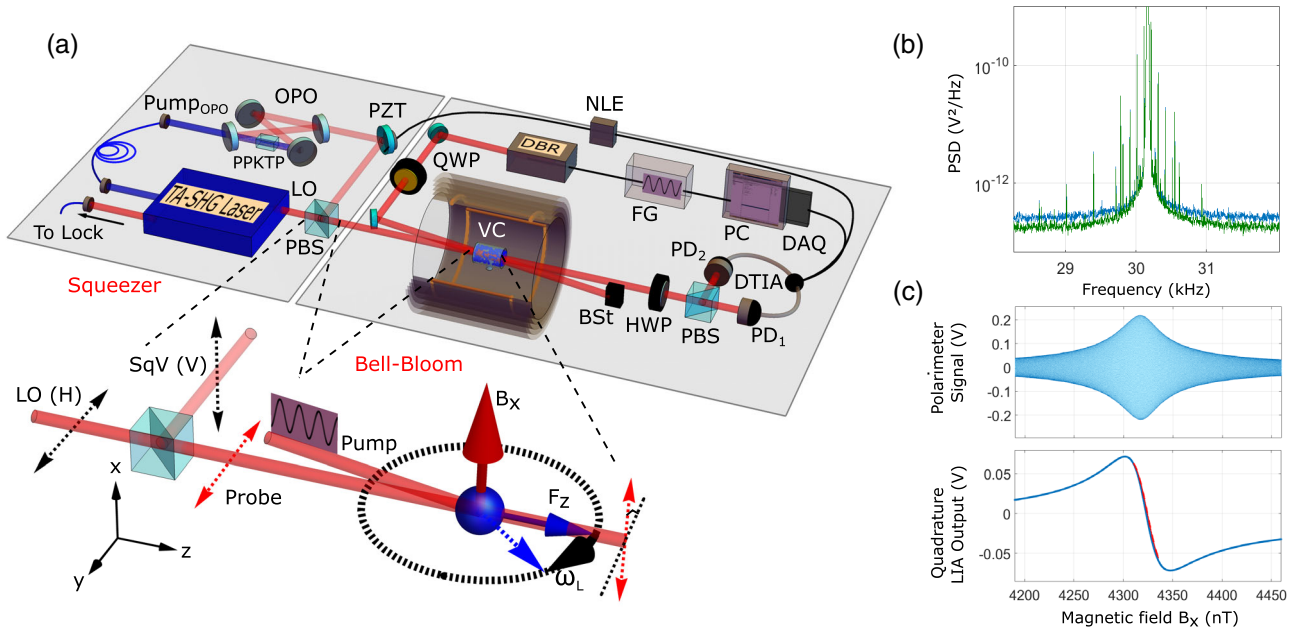

FIG. 1. Squeezed-light Bell-Bloom OPM. (a) Experimental setup. Tapered amplified second harmonic generator (TA-SHG); optical parametric oscillator (OPO); PPKTP, Nonlinear crystal; local oscillator (LO); polarizing beam splitter (PBS); quarter wave-plate (QWP); vapor cell (VC); beam stopper (BSt); half wave plate (HWP); photodiode (PD); differential transimpedance amplifier (DTIA); data acquisition (DAQ); function generator (FG); noise lock electronics (NLE). Bell-Bloom inset: Because of the magnetic field B_x atomic spins precess at the Larmor frequency ω_L in the transverse plane. Synchronously modulated optical pumping maintains the atomic spin polarization. A linearly polarized cw probe undergoes paramagnetic Faraday rotation. Squeezer inset: Vertically polarized squeezed vacuum is combined with horizontally polarized LO on a polarizing beam splitter to generate a polarization squeezed probe. (b) Power spectral density (PSD). Power spectrum of the BB signal for coherent and squeezed light around the Larmor frequency. The spectra are averages of 100 measurements, each one with duration of 0.5 sec. (c) Polarimeter signal (Top): Signal S_2 [Eq. (2)] for fixed pumping modulation frequency while scanning the magnetic field around resonance. OPM signal (bottom):—lock-in quadrature output (v) whose slope, calculated from the linear fit of the dispersive curve around the resonant field value, is used for the calibration of the magnetic sensitivity.

The experimental setup and coordinate system are shown in Fig. 1(a). Isotopically enriched ^{87}Rb vapor and 100 Torr of N_2 buffer gas are contained in a cell with interior length 3 cm. The cell, within a ceramic oven, is maintained by intermittent Joule heating at 105 °C to create a ^{87}Rb density of 8.2×10^{12} atoms/cm^3 and an optical transmission of about 70% for probe light blue detuned by 20 GHz from the D_1 line. The cell and heater sit at the center of four layers of cylindrical mu-metal shielding with cylindrical coils to control the bias field components B_α and gradients $\partial B_\alpha/\partial_z$, $\alpha \in \{x, y, z\}$. A 500 μW pump beam from a distributed Bragg reflector (DBR) laser, circularly polarized and current tunable within the D_1 line at 795 nm, propagates through the cell at a small angle from the z axis. An extended cavity diode laser at 795 nm is stabilized 20 GHz to the blue from the ^{87}Rb D_1 line with a fiber interferometer [33] and frequency doubled to produce violet light at 397.4 nm (Toptica TA-SHG 110). The violet light is mode cleaned in a polarization-maintaining fiber and then pumps a subthreshold optical parametric oscillator to produce vertically polarized squeezed vacuum at the laser fundamental frequency, as described in Ref. [34]. The squeezed vacuum is combined on a polarizing beam splitter with a mode-matched, horizontally polarized "local oscillator" (LO) laser beam at 795 nm to produce the polarization-squeezed probe. The relative phase between LO and squeezed vacuum is controlled by a piezoelectric actuator and active feedback using the broadband noise level of the signal as the system variable [34]. In both coherent and squeezed-light probing, a 400 μW beam is detected with a shot-noise-limited balanced polarimeter after the cell. The system is operated as a BB OPM at a finite field B = 4.3 μT by applying a low-noise current through the coils (current source Twinleaf CSUA300); gradients and other bias components are nulled. The DBR laser's current is square modulated with a duty cycle of 10% at angular frequency $\Omega = \omega_L \approx 2\pi \times 30$ kHz, equal to the angular Larmor frequency ω_L. The effect of the current modulation is to bring the laser frequency into optical resonance with the $F = 1 \rightarrow F' = 1, 2$ transitions once per modulation cycle. In each measurement cycle, the modulated pumping is maintained for 0.5 s. The resulting spin dynamics are observed as paramagnetic Faraday rotation of the probe beam. Under continuous, modulated pumping, the polarimeter signal oscillates with frequency Ω, and shows noise from both spin projection noise and photon shot noise [35].

The role of quantum noise can be qualitatively understood from a Bloch equation model described in detail in the Supplemental Material [36]. The spins evolve according to the stochastic differential equation $d\mathbf{F}/dt = \mathbf{V} + \mathbf{N}$, where $\mathbf{F}$ is the collective atomic spin vector, $\mathbf{N}$ is a Langevin noise term and

$$\mathbf{V} = -\gamma B\hat{x} \times \mathbf{F} - \Gamma\mathbf{F} + P(\hat{z}F_{\max} - \mathbf{F}) \tag{1}$$

is the drift rate [36]. Here γ is the gyromagnetic ratio of ^{87}Rb, $\Gamma = 1/T_2$ is the transverse relaxation rate, P is the optical pumping rate, $F_{\max} = N_A F$ is the maximum possible polarization, and N_A is the atom number. Equation (1) describes a spin oscillator with resonant frequency $\omega_L \equiv \gamma B = \gamma(B^{(0)} + B^{(1)})$, where $B^{(0)}$ is the time average of B and $|B^{(1)}| \ll |B^{(0)}|$.

In the small-angle approximation appropriate here, the Faraday rotation signal can be written as [37]

$$S_2 = GS_1F_z + N_{S_2}, \tag{2}$$

where S_α, $\alpha \in \{1, 2, 3\}$ indicate Stokes parameters at the output of the cell, G is a coupling constant, and N_{S_2} is the polarization noise of the detected Stokes component, a manifestation of quantum vacuum fluctuations [15].

The oscillating spins and signal can be described in terms of slowly varying quadratures ρ, σ, u, v via $F_z(t) = \rho\cos\Omega t + \sigma\sin\Omega t$ and $S_2(t) = u\cos\Omega t + v\sin\Omega t$. The in-phase ($u$) and quadrature ($v$) components are obtained by digital lock-in detection of the signal S_2. We set $\Omega = \gamma B^{(0)}$ to maximize u, at which point v is linear in $B^{(1)}$. Small changes in B produce a linear change in the phase of the S_2 oscillation, such that $\tilde{v}(\omega) = R(\omega)\tilde{B}(\omega)$, where a tilde indicates a Fourier amplitude,

$$R(\omega) \equiv \frac{\gamma\langle u\rangle}{-i\omega + \Delta\omega}, \tag{3}$$

is the magnetic response, $\langle u\rangle = GS_1^{(\mathrm{in})}\langle\rho\rangle$ is the signal amplitude, $\langle\rho\rangle$ is the equilibrium spin polarization, and $\Delta\omega \equiv \Gamma + \bar{P}$ is the response bandwidth, where $\bar{P}$ is the cycle average of P. We compute the single-sided power spectral density of this signal, as $\mathcal{S}_v(\omega) \equiv |\mathcal{F}[N_v]|^2$, where $\mathcal{F}$ is the discrete Fourier transform implemented with a Hann window.

The spin noise is

$$\mathbf{N} = \mathbf{N}_F + GS_3\hat{z} \times \mathbf{F}, \tag{4}$$

where $\mathbf{N}_F$ accounts for the noise introduced by pumping and relaxation, as required by the fluctuation-dissipation theorem [36], $GS_3\hat{z}$ is the effective field produced by ac-Stark shifts [38] due to the probe, and is effectively white.

The three quantum noise sources affect differently the measurement. The azimuthal projection of $\mathbf{N}_F$ contributes directly to the spin angle θ, just as would a magnetic field, and thus with efficiency $\propto R(\omega)$. In contrast, N_{S_2} is white noise, unrelated to the atomic response. Spectra of these two noise sources are shown in Fig. 2(a) along with the experimentally measured magnetic response for comparison. The weak noise term $GS_3\hat{z}$ competes with the stronger $|B|\hat{x}$ in directing the spin precession, such that only its Ω-resonant component has a first-order effect. Said effect only alters the F_x component, which has no first order effect on the signal S_2. As a result, this BB magnetometer is backaction evading [24,39,40]. Most importantly for the use of squeezed light, there is no deleterious effect from using squeezing to reduce the noise in S_2. While this necessarily increases the noise in S_3, said increase has no effect on the signal. Two potential benefits of optical squeezing are thus clear: it will reduce the noise for higher

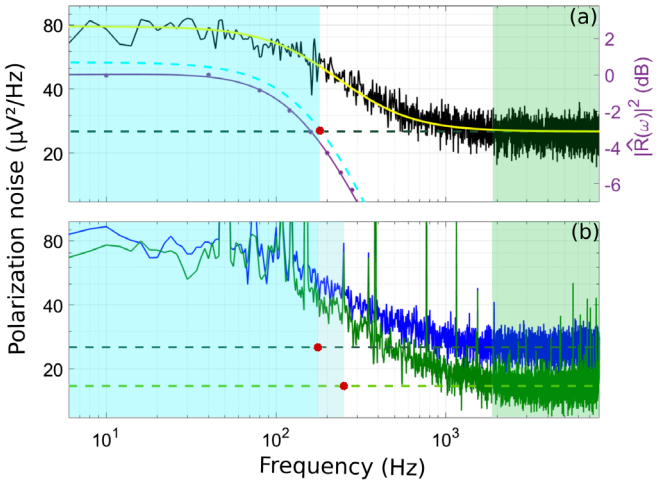

FIG. 2. Polarization rotation noise after demodulation. (a) Spin noise for unpolarized atoms. We fit the spectrum (black) with a model function of Eq. (S45) to estimate the response bandwidth, the photon shot noise (dashed green line) and the low frequency spin projection noise. Subtracting the constant shot noise contribution from the fitted combined noise (yellow) we infer the spin projection noise curve in the unpolarized state probed (dashed cyan). These noise levels define the spin projection noise (cyan) and photon shot noise (green) limited areas and the intermediate transition region (white). Purple dots and curve show, on the right axis, the measured normalized frequency response $|\hat{R}(\omega)|^2$ to an applied B_x modulation, and its fit with Eq. (3) with best fit parameter $\Delta\omega = 170$ Hz. (b) Magnetometer noise for polarized atoms. With 500 μW of pump power, the noise spectrum of the magnetometer shows a very similar behaviour to the unpolarized spectrum and apart from the technical noise peaks at the power-line frequency and harmonics, quantum noise is dominant. At high frequencies, the noise level is reduced by 1.9 dB for squeezed-light (green), with respect to the coherent (blue) probing. The dashed lines and the red dots depict estimates of photon shot noise level and cross-over frequencies when the squeezer is on and off, respectively.

frequencies, and increase the frequency at which the noise $S_v(\omega)$ transitions from spin-noise dominated to photon shot-noise dominated. As we describe below, this improves both high-frequency sensitivity and measurement bandwidth of this quantum-noise-limited sensor.

The calculation of magnetic sensitivity requires the above noise contributions to be normalized by the magnetic response. The latter is shown experimentally in Fig. 2(a), and via the BB noise model [36] to have a characteristic roll-off described by a Lorentzian $\mathcal{L}(\omega) = (\Delta\omega)^2/(\omega^2 + (\Delta\omega)^2)$ [24]. The magnetic noise density is then

$$\mathcal{S}_B(\omega) = \mathcal{S}_v(\omega)|R(\omega)|^{-2} = \frac{\Delta\omega^2}{\gamma^2\langle u\rangle^2}\left(\mathcal{S}_\sigma + \frac{1}{\mathcal{L}(\omega)}\mathcal{S}_{N_{S_2}}\right), \quad (5)$$

where $\mathcal{S}_\sigma$ and $\mathcal{S}_{N_{S_2}}$ are the noise spectral densities of the quadrature components of F and N_{S_2}, respectively, and are frequency independent. $\mathcal{S}_B(\omega)$ is nearly constant in the spin projection noise limited region and increases quadratically with frequency to double the low-frequency value at $\omega_{3\,\mathrm{dB}} \equiv \Delta\omega\sqrt{\mathcal{S}_\sigma/\mathcal{S}_{N_{S_2}} + 1}$. This frequency defines the 3 dB measurement bandwidth and grows with decreasing $\mathcal{S}_{N_{S_2}}$.

To demonstrate these advantages, we implement continuous-wave squeezed-light probing of the quantum-noise-limited BB OPM by using the experimental setup shown in Fig. 1(a). As already described, the resulting optical beam is horizontally polarized with squeezed fluctuations in the diagonal basis, i.e., squeezed in S_2. For an OPO pump power of 40.6 mW the generated polarization squeezing is at 2.4 dB before the cell, as measured from the PSD of the signal from an auxiliary balanced polarimeter. Because of 30% absorption losses, 1.9 dB of squeezing is observed in the PSD of both the BB polarimeter signal, shown in Fig. 1(b), and the demodulated quadrature component, shown in Fig. 2(b).

We compute the experimental sensitivity following prior work on BB magnetometers [25,41,42], as

$$\mathcal{S}_B(\omega) = \left(\frac{dv}{dB}\right)^{-2}\frac{\mathcal{S}_v(\omega)}{|\hat{R}(\omega)|^2}, \quad (6)$$

where $\mathcal{S}_v(\omega)$ is the observed noise in the lock-in quadrature component v, dv/dB is the slope of the quadrature signal and $|\hat{R}(\omega)|^2 \equiv |R(\omega)/R(0)|^2$ is the normalized frequency response of the spins to a modulation of the field B_x, shown in Figs. 2(b),1(c), and 2(a), respectively. Measurement of the magnetometer frequency response to a fixed amplitude sine wave magnetic field modulation in the range of 10 Hz to 2.4 kHz is used to experimentally determine $|R(\omega)|^2$ [36].

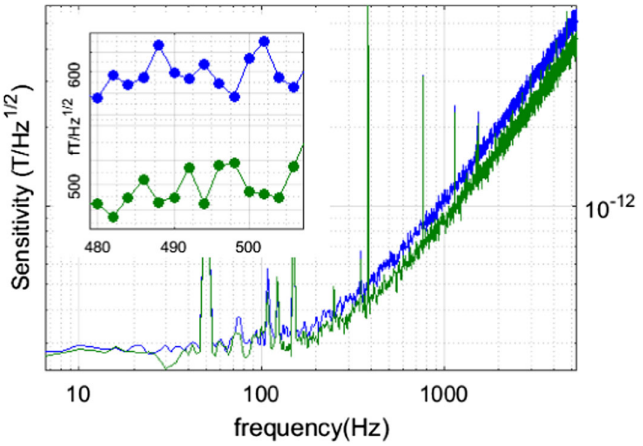

FIG. 3. Magnetic sensitivity. Sensitivity spectra for BB magnetometer probed with coherent (blue) and squeezed light (green). All data acquired with $P_{\mathrm{probe}} = 400\ \mu$W, $P_{\mathrm{pump}} = 500\ \mu$W, $T = 105\,^\circ$C, $n = 8.2 \times 12$ atoms/cm^3, $B_0 = 4.3\ \mu$T, $f_{\mathrm{mod}} = 30.164$ kHz. Polarization squeezing was 2.4 dB before the atomic cell and 1.9 dB at the detectors.

Turning on the squeezer causes $\mathcal{S}_{N_{S_2}}$ to drop to ξ^2 times its coherent-state value $\mathcal{S}^{\mathrm{SQL}}_{N_{S_2}}$, where ξ^2 is the squeezing parameter [43,44]. The predicted magnetic power spectral density is then

$$\mathcal{S}_B(\omega) = \frac{\Delta\omega^2}{\gamma^2\langle u\rangle^2}\left[\mathcal{S}_\sigma + \frac{\xi^2}{\mathcal{L}(\omega)}\mathcal{S}^{\mathrm{SQL}}_{N_{S_2}}\right] = \mathcal{S}^{\mathrm{SQL}}_B(\omega)\frac{1 + \mathcal{L}(\omega)\xi^2\zeta^{-2}}{1 + \mathcal{L}(\omega)\zeta^{-2}}, \quad (7)$$

where $\zeta^2 \equiv \mathcal{S}_\sigma/\mathcal{S}^{\mathrm{SQL}}_{N_{S_2}}$.

The enhancement due to squeezing is evident in the high frequency part of the experimental spectrum, shown in Fig. 3. At the detection frequency of 490 Hz, a polarization squeezing of 1.9 dB results in a 17% quantum enhancement of magnetic sensitivity, from 600 fT/$\sqrt{\mathrm{Hz}}$ down to 500 fT/$\sqrt{\mathrm{Hz}}$. As seen in Fig. 3, squeezing does not add noise to any region of the spectrum. This is a direct experimental demonstration that the BB technique evades backaction associated with the antisqueezed S_3 component.

Squeezed-light probing also increases the 3 dB measurement bandwidth [24]. For the data presented in Fig. 3, the original measurement bandwidth of 275 Hz is already higher than the response bandwidth $\Delta\omega = 170$ Hz and it is further increased to 320 Hz, with about 15% of quantum enhancement. This result agrees with the predicted improved 3 dB measurement bandwidth estimated via

$$\omega^{\mathrm{sq}}_{3\,\mathrm{dB}} = \omega^{\mathrm{SQL}}_{3\,\mathrm{dB}}\sqrt{\frac{1 + \zeta^2\xi^{-2}}{1 + \zeta^2}}. \quad (8)$$

The quantum advantages demonstrated here are limited by the squeezing produced by our OPO [34], and by probe transmission losses. Optical losses for the probe can, in principle, be made arbitrarily small without altering the other characteristics of the magnetometer, by increasing the probe detuning while boosting the probe power to keep constant the probe power broadening. More recent OPO designs [45,46] have demonstrated up to 15 dB of squeezing.

In conclusion, we have demonstrated that a polarization-squeezed probe can give both higher sensitivity and larger measurement bandwidth in a sensitive optically pumped magnetometer. In contrast to squeezed-light probing of optomechanical sensors such as gravitational wave detectors [47], the sensitivity advantage at high frequencies comes without the cost of increased backaction noise at low frequencies. This occurs because QND measurement of a precessing spin system shunts backaction effects into the unmeasured spin degree of freedom [39], something not possible in a canonical system such as a mechanical oscillator [48]. Squeezed-light probing is compatible with and complementary to other methods to enhance sensitivity and bandwidth, including spin-exchange relaxation suppression [49], pulsed geometries [30,31], multipass geometries [26], Kalman filtering [50] and closed-loop techniques [29].

We thank Michele Gozzelino and Dominic Hunter for laboratory assistance and helpful discussions and Vindhiya Prakash for feedback on the manuscript. This project was supported by H2020 Future and Emerging Technologies Quantum Technologies Flagship projects MACQSIMAL (Grant Agreement No. 820393) and QRANGE (Grant Agreement No. 820405); H2020 Marie Skłodowska-Curie Actions projects ITN ZULF-NMR (Grant Agreement No. 766402) and PROBIST (Grant Agreement No. 754510), Spanish Ministry of Science projects OCARINA (PGC2018-097056-B-I00 project funded by MCIN/ AEI /10.13039/501100011033/ FEDER "A way to make Europe") and "Severo Ochoa" Center of Excellence CEX2019-000910-S Generalitat de Catalunya through the CERCA program; Agència de Gestió d'Ajuts Universitaris i de Recerca Grant No. 2017-SGR-1354; Secretaria d'Universitats i Recerca del Departament d'Empresa i Coneixement de la Generalitat de Catalunya, co-funded by the European Union Regional Development Fund within the ERDF Operational Program of Catalunya (project QuantumCat, ref. 001-P-001644); Fundació Privada Cellex; Fundació Mir-Puig, J. K. acknowledges the support from NSFC through Grants No. 11935012, No. 12005049.

*Corresponding author.
charikleia.troullinou@icfo.es

†Corresponding author.
jia.kong@hdu.edu.cn

[1] D. Budker and M. Romalis, Nat. Phys. **3**, 227 (2007).
[2] W. Happer, Rev. Mod. Phys. **44**, 169 (1972).
[3] H. B. Dang, A. C. Maloof, and M. V. Romalis, Appl. Phys. Lett. **97**, 151110 (2010).
[4] E. Boto, N. Holmes, J. Leggett, G. Roberts, V. Shah, S. S. Meyer, L. D. Muñoz, K. J. Mullinger, T. M. Tierney, S. Bestmann, G. R. Barnes, R. Bowtell, and M. J. Brookes, Nature (London) **555**, 657 (2018).
[5] C. Abel *et al.*, Phys. Rev. Lett. **124**, 081803 (2020).
[6] S. Knappe, V. Gerginov, P. D. Schwindt, V. Shah, H. G. Robinson, L. Hollberg, and J. Kitching, Opt. Lett. **30**, 2351 (2005).
[7] T. W. Kornack, R. K. Ghosh, and M. V. Romalis, Phys. Rev. Lett. **95**, 230801 (2005).
[8] J. Lee, A. Almasi, and M. Romalis, Phys. Rev. Lett. **120**, 161801 (2018).
[9] M. E. Limes, D. Sheng, and M. V. Romalis, Phys. Rev. Lett. **120**, 033401 (2018).
[10] S. F. Huelga, C. Macchiavello, T. Pellizzari, A. K. Ekert, M. B. Plenio, and J. I. Cirac, Phys. Rev. Lett. **79**, 3865 (1997).
[11] M. Auzinsh, D. Budker, D. F. Kimball, S. M. Rochester, J. E. Stalnaker, A. O. Sushkov, and V. V. Yashchuk, Phys. Rev. Lett. **93**, 173002 (2004).
[12] T. Horrom, R. Singh, J. P. Dowling, and E. E. Mikhailov, Phys. Rev. A **86**, 023803 (2012).
[13] I. Novikova, E. E. Mikhailov, and Y. Xiao, Phys. Rev. A **91**, 051804 (2015).
[14] G. Vasilakis, V. Shah, and M. V. Romalis, Phys. Rev. Lett. **106**, 143601 (2011).
[15] C. M. Caves, Phys. Rev. D **23**, 1693 (1981).
[16] P. Grangier, R. E. Slusher, B. Yurke, and A. LaPorta, Phys. Rev. Lett. **59**, 2153 (1987).
[17] E. S. Polzik, J. Carri, and H. J. Kimble, Phys. Rev. Lett. **68**, 3020 (1992).
[18] Y. Han, X. Wen, J. He, B. Yang, Y. Wang, and J. Wang, Opt. Express **24**, 2350 (2016).
[19] F. Wolfgramm, A. Cerè, F. A. Beduini, A. Predojević, M. Koschorreck, and M. W. Mitchell, Phys. Rev. Lett. **105**, 053601 (2010).
[20] N. Otterstrom, R. C. Pooser, and B. J. Lawrie, Opt. Lett. **39**, 6533 (2014).
[21] I. Novikova, E. E. Mikhailov, and Y. Xiao, Phys. Rev. A **91**, 051804(R) (2015).
[22] X. Zhang, S. Jin, W. Qu, and Y. Xiao, Appl. Phys. Lett. **119**, 054001 (2021).
[23] W. E. Bell and A. L. Bloom, Phys. Rev. Lett. **6**, 280 (1961).
[24] V. Shah, G. Vasilakis, and M. V. Romalis, Phys. Rev. Lett. **104**, 013601 (2010).
[25] V. Gerginov, M. Pomponio, and S. Knappe, IEEE Sens. J. **20**, 12684 (2020).
[26] D. Sheng, S. Li, N. Dural, and M. V. Romalis, Phys. Rev. Lett. **110**, 160802 (2013).
[27] V. G. Lucivero, W. Lee, N. Dural, and M. V. Romalis, Phys. Rev. Applied **15**, 014004 (2021).
[28] A. R. Perry, M. D. Bulatowicz, M. Larsen, T. G. Walker, and R. Wyllie, Opt. Express **28**, 36696 (2020).
[29] R. Li, F. N. Baynes, A. N. Luiten, and C. Perrella, Phys. Rev. Applied **14**, 064067 (2020).

[30] V. G. Lucivero, W. Lee, M. V. Romalis, M. E. Limes, E. L. Foley, and T. W. Kornack, Quantum information and measurement (QIM) V: Quantum technologies, Rome, Italy, OSA Technical Digest, T3C. 3, 2019.
[31] M. E. Limes, E. L. Foley, T. W. Kornack, S. Caliga, S. McBride, A. Braun, W. Lee, V. G. Lucivero, and M. V. Romalis, Phys. Rev. Applied **14**, 011002(R) (2020).
[32] M. W. Mitchell and S. Palacios Alvarez, Rev. Mod. Phys. **92**, 021001 (2020).
[33] J. Kong, V. G. Lucivero, R. Jiménez-Martínez, and M. W. Mitchell, Rev. Sci. Instrum. **86**, 073104 (2015).
[34] A. Predojević, Z. Zhai, J. M. Caballero, and M. W. Mitchell, Phys. Rev. A **78**, 063820 (2008).
[35] V. G. Lucivero, P. Anielski, W. Gawlik, and M. W. Mitchell, Rev. Sci. Instrum. **85**, 113108 (2014).
[36] See Supplemental Material at http://link.aps.org/supplemental/10.1103/PhysRevLett.127.193601 for more details.
[37] J. Kong, R. Jiménez-Martínez, C. Troullinou, V. G. Lucivero, G. Tóth, and M. W. Mitchell, Nat. Commun. **11**, 2415 (2020).
[38] W. Happer and B. S. Mathur, Phys. Rev. **163**, 12 (1967).
[39] G. Colangelo, F. M. Ciurana, L. C. Bianchet, R. J. Sewell, and M. W. Mitchell, Nature (London) **543**, 525 (2017).
[40] G. Colangelo, F. Martin Ciurana, G. Puentes, M. W. Mitchell, and R. J. Sewell, Phys. Rev. Lett. **118**, 233603 (2017).
[41] R. Jiménez-Martínez, W. C. Griffith, S. Knappe, J. Kitching, and M. Prouty, J. Opt. Soc. Am. B **29**, 3398 (2012).
[42] V. Gerginov, S. Krzyzewski, and S. Knappe, J. Opt. Soc. Am. B **34**, 1429 (2017).
[43] V. G. Lucivero, R. Jiménez-Martínez, J. Kong, and M. W. Mitchell, Phys. Rev. A **93**, 053802 (2016).
[44] V. G. Lucivero, A. Dimic, J. Kong, R. Jiménez-Martínez, and M. W. Mitchell, Phys. Rev. A **95**, 041803(R) (2017).
[45] Y. Han, X. Wen, J. He, B. Yang, Y. Wang, and J. Wang, Opt. Express **24**, 2350 (2016).
[46] H. Vahlbruch, M. Mehmet, K. Danzmann, and R. Schnabel, Phys. Rev. Lett. **117**, 110801 (2016).
[47] L. McCuller, C. Whittle, D. Ganapathy, K. Komori, M. Tse, A. Fernandez-Galiana, L. Barsotti, P. Fritschel, M. MacInnis, F. Matichard, K. Mason, N. Mavalvala, R. Mittleman, H. Yu, M. E. Zucker, and M. Evans, Phys. Rev. Lett. **124**, 171102 (2020).
[48] Q. Y. He, S.-G. Peng, P. D. Drummond, and M. D. Reid, Phys. Rev. A **84**, 022107 (2011).
[49] I. M. Savukov, Spin exchange relaxation free (SERF) magnetometers, in *High Sensitivity Magnetometers*, edited by A. Grosz, M. J. Haji-Sheikh, and S. C. Mukhopadhyay (Springer International Publishing, Cham, 2017), pp. 451–491.
[50] R. Jiménez-Martínez, J. Kołodyński, C. Troullinou, V. G. Lucivero, J. Kong, and M. W. Mitchell, Phys. Rev. Lett. **120**, 040503 (2018).